Salt-penetrating and non-salt-penetrating tear faults in central Tarim Basin

Qing Bian[1], Zhendong Wang[1,2,3]

[1]Petroleum Exploration and Production Research Institute, Sinopec, Beijing, China,

[2]National Energy Laboratory of Carbonate Oil and Gas, Sinopec, Beijing, China,

[3]Key Laboratory of Deep Geology and Resources, Sinopec, Beijing, China

Corresponding author: Qing Bian (bianqing.syky@sinopec.com)

Key Points:

- High-resolution seismic coherence maps were extracted clearly showing No. 4 Fault penetrated salt and No. 7 Fault terminated in salt

- Strata shortening data of Nos. 4 and 7 Faults were calculated to explain why No. 4 Fault can penetrate salt while No. 7 Fault cannot

- A lack of shortening difference in the sub-salt strata implies that a tear fault cannot penetrate the salt layer

Abstract

We examined two tear faults, namely, Nos. 4 and 7 Faults, in Tarim Basin to investigate how a tear fault penetrates the salt layer. Using high-quality seismic data, we showed that No. 4 Fault penetrates the salt layer, whereas No. 7 Fault does not. We calculated the strata shortening data of Nos. 4 and 7 Faults. For No. 4 Fault, we observed shortening differences between the western and eastern sections in both the supra- and sub-salt strata, whereas for No. 7 Fault, we observed shortening differences only in the supra-salt strata. We demonstrated that under the action of thrusting, a tear fault could penetrate the salt layer if there is a shortening difference in the different positions of the sub-salt strata. A lack of shortening difference in the sub-salt strata implies that a tear fault cannot penetrate the salt layer, even though the sub-salt strata are deformed during thrusting.

Plain Language Summary

Tear fault is a kind of steeply dip strike-fault caused by adjusting the displacement gap in the process of thrust. This paper deals with the problem of how deep a tear fault can extend downward. Due to the lack of deep data, previous studies on this problem mainly inferred indirectly from the evidence of outcrop scale. In this paper, high quality seismic data are used to clearly show whether two tearing faults, namely, Nos. 4 and 7 Faults, in the Tarim Basin can pass through the deep salt layer. Then, through the calculation of strata shortening, we prove that the sub-salt strata of No. 7 Fault did not have the original driving force to form the tear fault, while the sub-salt strata of No. 4 Fault were torn to form the tear fault.

1 Introduction

Tear faults are a common geological phenomenon on Earth and have been studied worldwide, for example, the Appalachian orogenic belt in West Virginia (Wheeler, 1980), Zagros orogenic belt in Iran (Jahani et al., 2017), north-eastern Maracaibo Basin in Venezuela (Escalona & Mann, 2006), and Niger Delta in Africa (Benesh et al., 2014). One aspect in the study of tear faults is evaluating how deep the tear fault can extend. In 1980, Wheeler's studied the downward progression of Parsons and Petersburg Lineaments in West Virginia, and assumed that they did not cut the basement. Wheeler cited evidence for surface mapping and gravity data; however, this evidence was indirect. In conclusion, Wheeler could not determine whether Parsons and Petersburg Lineaments passed through the deep detachment layer (Wheeler, 1980). Another study in the Burro Negro fault zone, based on outcrop and two-dimensional seismic data, suggested that the Burro Negro fault penetrated the salt layer (Escalona & Mann, 2006). However, outcrop observations do not provide adequate insights into subsurface conditions, and in practice, seismic interpretation is a blend of science and art (Jackson & Hudec, 2017) when the quality of seismic data is substandard. Based on outcrops, two-dimensional seismic data, and the focal depth of natural earthquakes, Jahani et al. (2017) suggested that a tear fault in the Zagros thrust belt did not penetrate the Hormuz salt layer; however, their calculation of the source depth of natural earthquakes may have contained errors. In general, the constriction on whether the tear fault can penetrate salt is mainly due to the poor quality of deep-earth data. Estimating the depth of a tear fault and evaluating why

some tear faults cut through the deep salt (detachment layer) and others end at the salt

layer are practically challenging.

This problem can effectively be solved using high-quality seismic data that can

cover the development depth of a tear fault. In this study, we selected Nos. 4 and 7

tear faults in the Shuntuoguole Low Uplift, Tarim Basin, as the research subjects.

Using high-resolution seismic data, we extracted the seismic coherence maps at

different depths, which clearly indicated that No. 4 Fault penetrated salt and No. 7

Fault terminated in salt. We then explain why No. 4 Fault could cut through the salt as

opposed to No. 7 Fault by analysing the strata shortening data.

2 Data and Methods

We used high-quality seismic data collected along Nos. 4 and 7 tear faults by

Sinopec. Both the trace and bin spacings for the seismic cube are approximately 25 m.

All seismic data were displayed in seconds, but the two-way-time-to-depth conversion

was conducted using a velocity of 5500 m/s. In the map view, seismic coherence

(Bahorich & Farmer, 1995) was used to image faults. Curvimetric and planimetric

shortenings were calculated to evaluate the strata movement (Laubscher, 1961;

Gonzalez-Mieres & Suppe, 2006).

3 Geological Setting

3.1 Tear faults in the Shuntuoguole Low Uplift

A series of tear faults has been observed in the Shuntuoguole Low Uplift. These

faults are vertical, ranging in length from tens to hundreds of kilometres, but with a

low slip distance. Sun et al. (2021) measured the slip distance of No. 5 Fault, which

81   was between 200 and 1520 m. These tear faults can be classified into two systems

82   according to the fault strike. The thrusting of the Katake Uplift resulted in the

83   formation of Nos. 4, 6, 8, 12, 16, and southern No. 5 faults. The strike of these faults

84   is NNE-SSW, perpendicular to the Tazhong No. 1 Fault. Another thrust-tear fault

85   system was formed in the northwest region of the Shuntuoguole Low Uplift, including

86   the northern part of No. 5 Fault and Nos. 7, 9, and 11 Faults. These faults are

87   distributed in the NNW-SSE direction, perpendicular to the strike of the Luntai fault

88   (Figure 1b). Considering the case of No. 5 Fault, Sun et al. (2021) studied the active

89   stages of the tear faults. These tear faults began to form under regional compression

90   during the middle Ordovician Period, and the entire thrust-tearing process lasted until

91   the late Ordovician Period. By the beginning of the Silurian Period, the regional

92   tectonic setting had become extensional (Sun et al., 2021).

93   3.2 Strata

94   Considering the tectonic setting, we focused on the Ordovician strata and those

95   below it. Mudstones are deposited in the Yuertusi Formation (Deng et al., 2021). In

96   the Xiaoerbulake Formation, the carbonate deposits are dominated by dolomite (Ji et

97   al., 2020; Deng et al., 2019). Salt layers include the Wusonggeer Formation and the

98   bottom of the Awatage Formation (Bian et al., 2022). The Shayilike Formation,

99   comprising limestone, is sandwiched between salt layers. The supra-salt assemblage

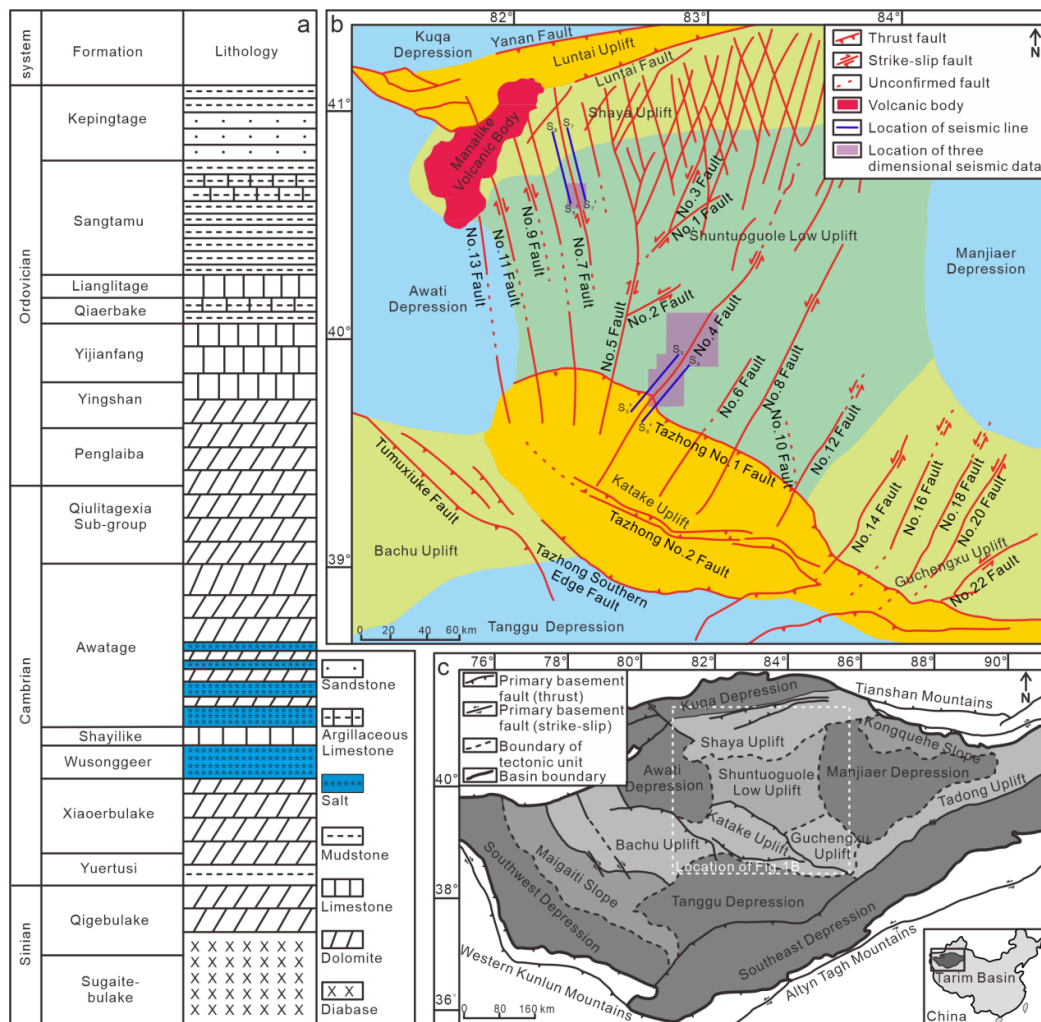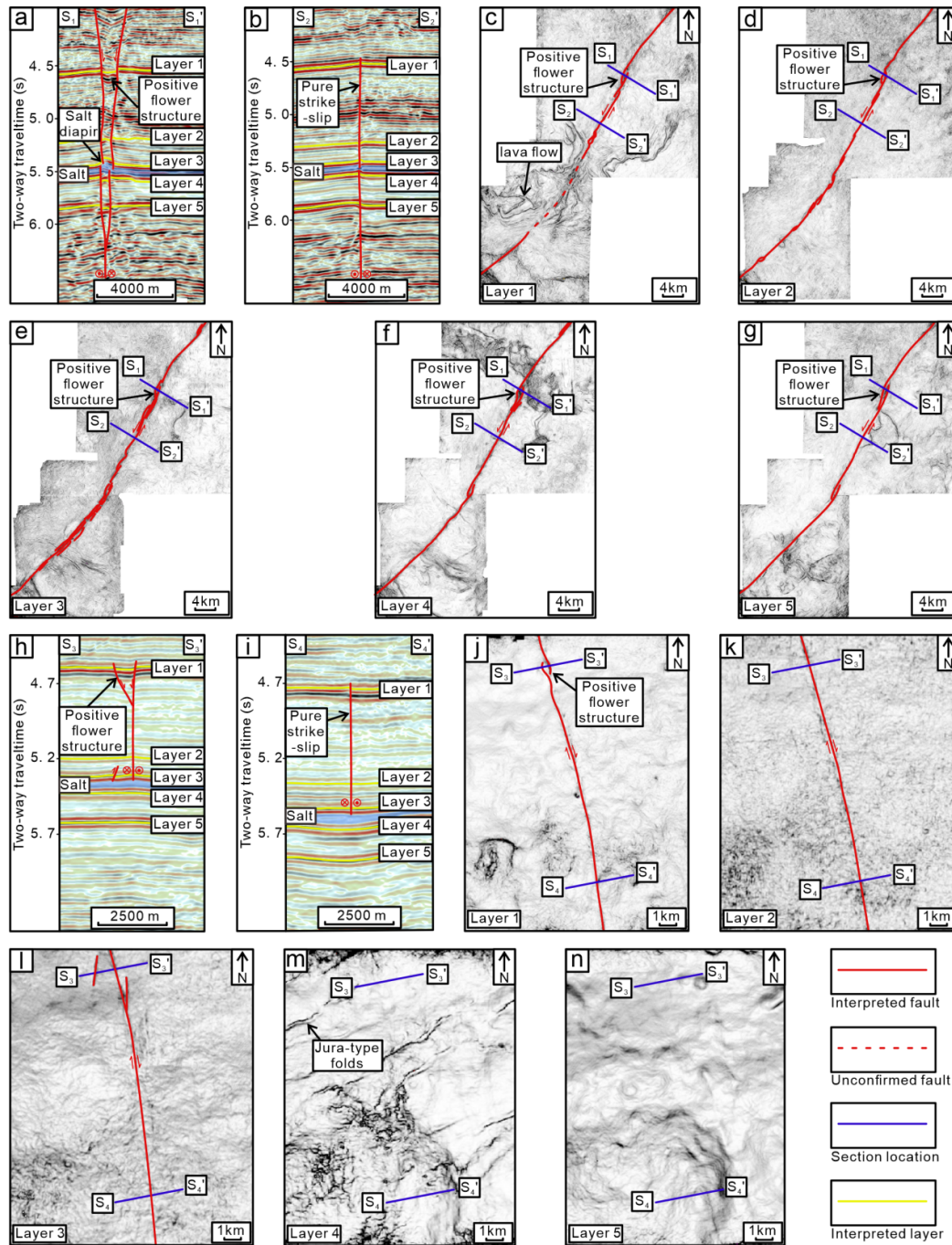100   comprises dolomite, limestone, mudstone, and sandstone (Figure 1a).

Figure 1. (a) The stratigraphy of Sinian, Cambrian, and Ordovician; (b) the distribution of faults in the Shuntuoguole Low Uplift (Figure 1c shows the locations). The faults are projected to the top of the Yijianfang Formation; (c) the structural units in the Tarim Basin.

4 Interpretation

4.1 Interpretation of No. 4 Fault

No. 4 Fault extends from the Katake Uplift to the Shuntuoguole Low Uplift. Its overall strike is NNE-SSW, perpendicular to that of the Tazhong No. 1 Fault. The fault strike is parallel to the southern parts of Nos. 5, 8, and 12 Faults (Figure 1b). We

Figure 2. (a), (b), (h), (i) Interpretation for sections S_1, S_2, S_3, and S_4 (Figures 2 (c)-(g) and (j)-(n) show the locations); vertical exaggeration of the section = 2. (c)-(g) Interpretation of the top of the Yijianfang Formation, top of the Awatage Formation, top and bottom of the Wusonggeer Formation, and the bottom of Yuertusi Formation's coherence slices in No. 4 Fault. (j)-(n) Interpretation of the top of the Yijianfang

117 Formation, top of the Awatage Formation, top and bottom of the Wusonggeer

118 Formation, and the bottom of Yuertusi Formation's coherence slices in No. 7 Fault.

119 Figure 1b shows the locations of seismic data.

120 obtained seismic coherence maps of five layers of No. 4 Fault at various depths.

121 Layers 1-5, respectively, cover the rigid strata above the salt, the top and bottom of

122 the salt, and the rigid strata below the salt. Traces of the strike-slip fault can be

123 observed in the five layers (Figures 2c–2g). For example, in section S_1, the fault

124 develops a positive flower structure (Figure 2a). In the rigid layers, the structure style

125 is consistent as the strata in the fault zone of layers 1, 2, and 5 collapsed. The seismic

126 coherence maps show that the left-stepping fault stepover is present at this position

127 (Figures 2c–2g). Accordingly, No. 4 Fault was evaluated to be a left-lateral fault

128 (Fossen, 2010). Layer 3, the top layer of the salt, is convex in this position, forming a

129 salt diapir, which is related to the low density and high rheology of salt (Bian et al.,

130 2022). In general, the interpretation results of section S_1 (Figures 2c–2g), indicate that

131 the sub-salt, salt, and supra-salt strata of No. 4 Fault are involved in a positive flower

132 structure at this position. Section S_2 displays pure strike-slip, and notably, the fault

133 penetrates the salt layer (Figure 2b). In summary, we determined that No. 4 Fault

134 penetrated the salt layer.

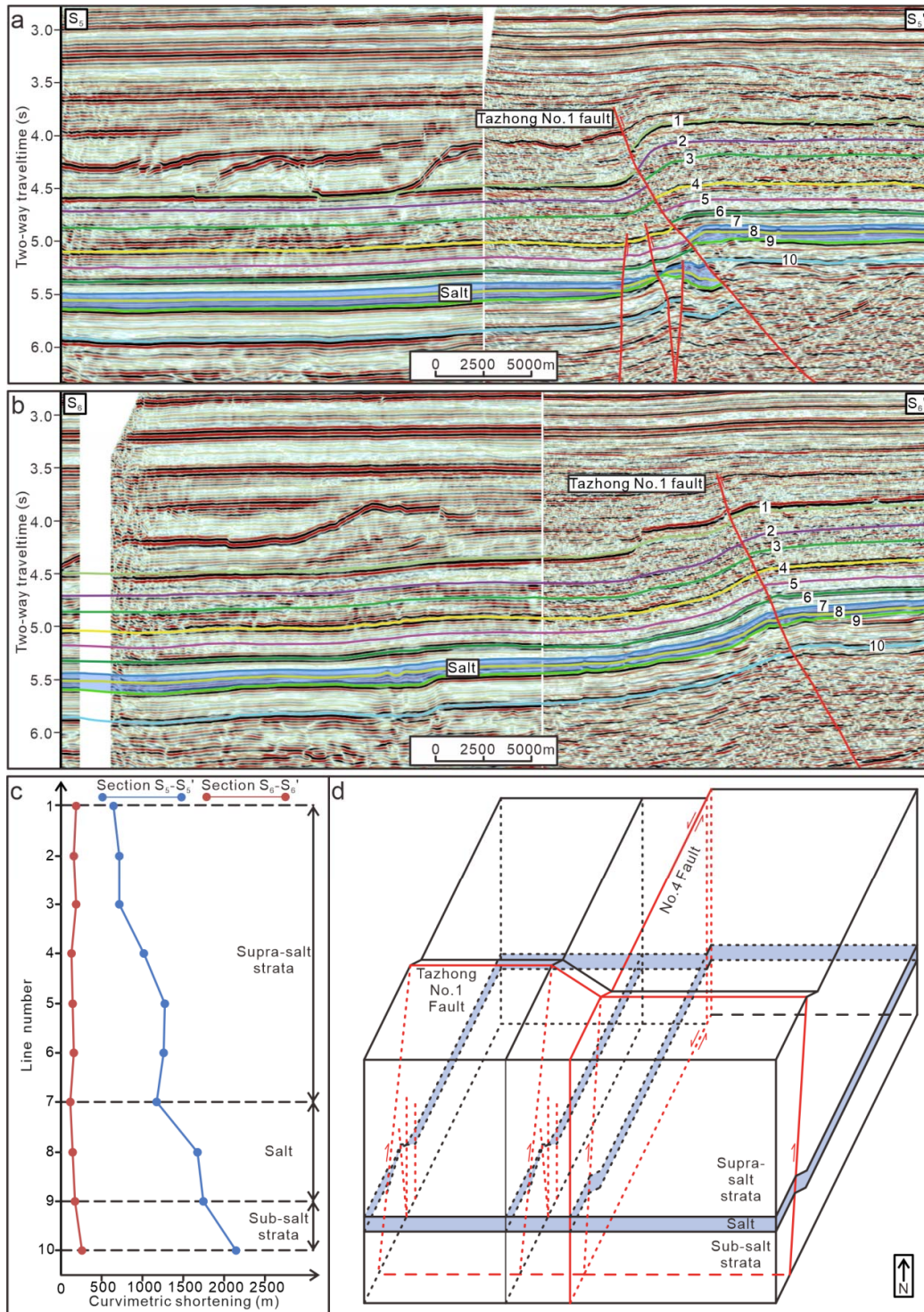135   4.2 Interpretation of No. 7 Fault

136   No. 7 Fault is an NNW-SSE trending tear fault developing in the northwest of the

137 Shuntuoguole Low Uplift, belonging to the thrust-tear fault system in the northwest

138 region of the Shuntuoguole Low Uplift (Figure 1b). Corresponding to the seismic

coherence maps of No. 4 Fault, we extracted five seismic coherence maps of No. 7

Fault (Figures 2j–2n). No. 7 Fault is dominated by pure strike-slip, and only a small

positive flower structure is observed in the northern part (Figure 2h). The positive

flower structure can only be recognised in Figure 2j, and when it is folded down, it

shows a linear distribution, as shown in Figure 2k. The positive flower structure

shows a right-step distribution pattern (Figure 2j); thus, No. 7 Fault is evaluated as a

right-lateral strike-slip fault (Fossen, 2010). No. 7 Fault is only shown in Figures 2j, k,

l, and no trace of a fault is found in Figure 2m, which shows NEE-SWW-trending

Jura-type folds. No fault was observed in sub-salt layer 5 (Figure 2n). In particular,

No. 7 Fault only developed in the strata above the salt layer but not below it. Thus, No.

7 Fault did not penetrate the salt.

5 Calculation and Results

To determine why No. 4 Fault penetrates the salt and No. 7 Fault terminates

above it, we must evaluate the cause of the tear fault. The tear fault is a strike-slip

fault that mediates the difference in the strata displacement in different parts of the

thrust system (Jackson & Hudec, 2017). Therefore, there was a difference in the strata

shortening parallel to the thrust on the two sides of the tear fault. If the shortening of a

block is consistent without a difference in displacement, no tear fault will be formed.

If we can measure and compare the thrust shortening amount of the sub- and

supra-salt strata on the two sides of the tear fault, we can determine why No. 4 Fault

penetrates the salt while No. 7 Fault does not.

5.1 Strata shortening on both sides of No. 4 Fault

Figure 3. (a)-(b) Interpretation for sections S_5 and S_6 (Figure 1b shows the location);

vertical exaggeration of the section = 2. (c) Curvimetric shortening in sections S_5, S_6.

(d) Schematic diagram showing No. 4 Fault penetrating the salt.

165 We intercepted two seismic sections on the east and west sides of No. 4 Fault to

166 elucidate formation shortening. The strike of the two seismic sections is parallel to

167 that of No. 4 Fault, and the sections are approximately 5 km away from No. 4 Fault.

168 Both sections cover the hanging wall and footwall of the Tazhong No.1 Fault. The

169 lengths of the two sections are consistent at 45435.24 m. We chose 10 lines in two

170 sections, including the supra-salt rigid, salt, and sub-salt strata. We measured and

171 calculated the curvimetric shortening of the 10 lines on both sides of No. 4 Fault.

172 In section S_5 (Figure 3a), the Tazhong No. 1 Fault cuts through the strata above

173 the salt, the salt layer, and strata below the salt, and obvious fault displacement is

174 observed in the 10 interpreted lines. When the salt is cut through, plastic flow occurs,

175 resulting in thinning and thickening of the salt. Simultaneously, three faults were

176 derived from the footwall of the Tazhong No. 1 Fault, and were developed at great

177 depths, namely, in the sub-salt strata, salt layer, and parts of the supra-salt strata. This

178 indicates that in section S_5, the Tazhong No. 1 Fault has strong activity, and the

179 supra-salt, salt, and sub-salt strata are all affected. In section S_6 (Figure 3b), the

180 deformation is gentle compared with that in section S_5. Section S_6 shows that the fault

181 displacement was small between the hanging wall and footwall of the Tazhong No. 1

182 Fault zone at this position. The thickness of the salt was stable. No secondary faults

183 were observed in the footwall, indicating that the thrusting of the Tazhong No. 1 Fault

184 does not cause obvious strata deformation at section S_6. In particular, the strata

185 deformation on the western side of No. 4 Fault is more obvious than that on the
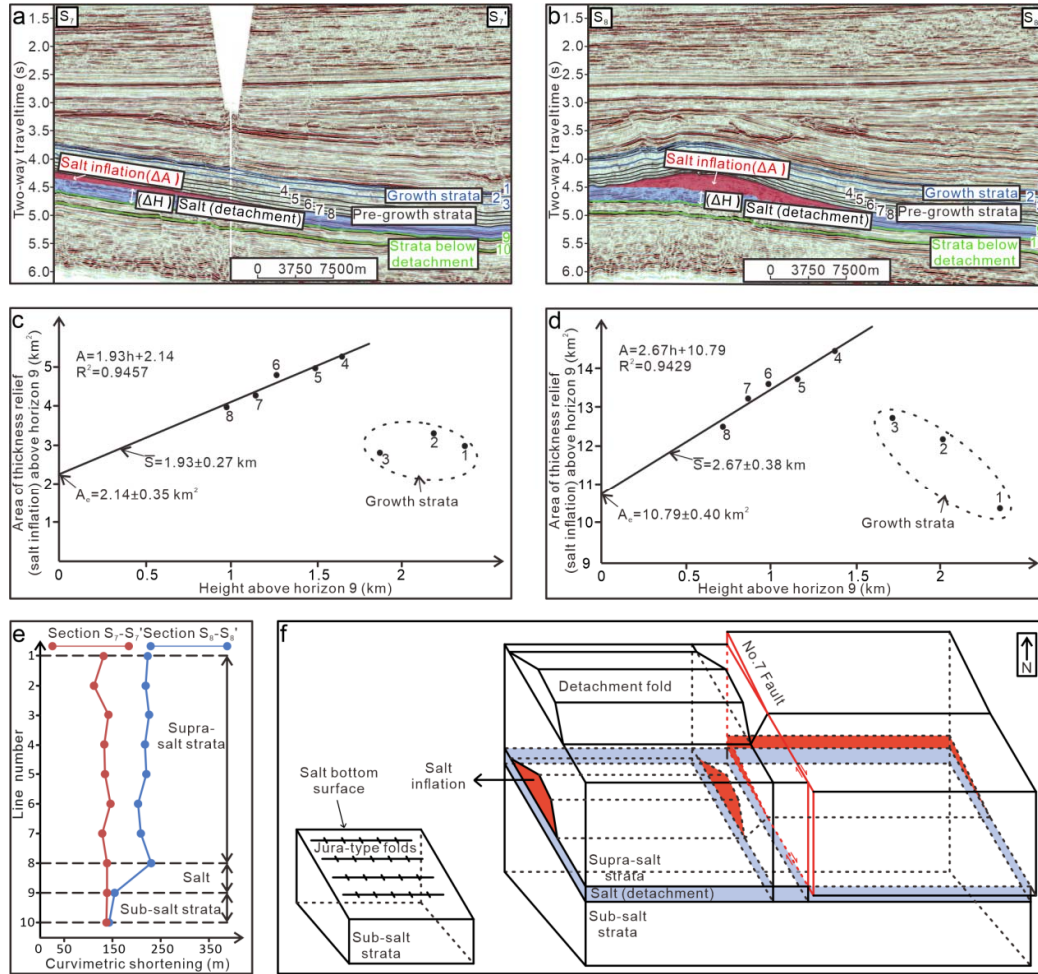
186 eastern side.

187   The curvimetric shortening data shows differences on both sides of No. 4 Fault

188   (Figure 3c). Overall, the curvimetric shortening of each line in section S_5 was greater

189   than that in section S_6, including the sub-salt (lines 9 and 10), inter-salt (line 8), and

190   supra-salt (lines 1–7) strata. Considering the supra-salt strata, the average curvimetric

191   shortening of lines 1–7 in section S_5 is 972.84 m, and that in section S_6 is 152.26 m,

192   with a difference of 820.58 m. Considering the sub-salt and inter-salt strata (lines 8–

193   10), the average curvimetric shortening of lines 8–10 in section S_5 is 1855.20 m, and

194   that in section S_6 is 193.28 m, with a difference of 1661.92 m.

195   Although the curvimetric shortening used here cannot accurately represent the

196   actual amount of shortening (Gonzalez-Mieres & Suppe, 2006), under the same

197   measurement standard, the curvimetric shortening reflects the difference in strata

198   shortening. The western wall of No. 4 Fault caused a greater shortening amount,

199   whereas its eastern wall had a smaller shortening amount. This difference explains

200   why the strata at No. 4 Fault formed a tear fault. The shortening amounts of the supra-

201   and sub-salt strata on both sides of No. 4 Fault are different; thus, both the supra- and

202   sub-salt strata are torn to form faults, which explains why the tear of No. 4 Fault cuts

203   through the salt (Figure 3d).

204   5.2 Strata shortening on both sides of No. 7 Fault

205   We obtained two seismic sections from the eastern and western sides of No. 7

206   Fault to measure the formation shortening. The strike of the two seismic sections was

207   parallel to that of No. 7 Fault, and the sections were approximately 5 km away from

208   No. 7 Fault. The lengths of the two sections are the same, namely, 45435.85 m. We

209 chose 10 lines in two sections, covering the supra- to sub-salt strata.

Figure 4. (a)-(b) Interpretation for sections S_7 and S_8 (Figure 1b shows the location); vertical exaggeration of the section = 2. (c)-(d) Area of relief graph for sections S_7 and S_8. (e) Curvimetric shortening in sections S_7 and S_8. (f) Schematic diagram showing that No. 7 Fault did not penetrate the salt.

Section S_7 shows that the strata are relatively gentle overall and inclined in the southeast direction; there is a slight thickening of salt (salt inflation) on the northwest side of section S_7 (Figure 4a). Comparatively, the salt is obviously thickened in section S_8, leading to the detachment fold in the supra-salt strata, whereas the sub-salt strata are inclined in the southeast direction owing to regional thrusting (Figure 4b).

220   Owing to the presence of detachment folds, planimetric shortening was calculated

221   to recover the shortening of the supra-salt strata (lines 1–8). Line 9 was used as the

222   reference. Simultaneously, we also collected the curvimetric shortening data. Using

223   the sub-salt strata as the reference plane for measurement, we concluded that the

224   average planimetric shortening (referring line 9) of the supra-salt strata in section S_7 is

225   approximately 1.93 km (Figure 4c) and that in section H is 2.67 km (Figure 4d), with

226   a difference of 0.74 km. The supra-salt strata on the eastern and western sides of No. 7

227   Fault have displacement differences owing to thrusting, and this difference led to the

228   tearing of the supra-salt strata, forming a tear fault.

229   The average curvimetric shortening of the sub-salt strata (lines 9 and 10) in

230   section S_7 is 138.32 m, whereas that in section S_8 is 148.50 m. This shows that

231   although the strata were deformed beneath the salt, no significant displacement

232   difference was observed between the eastern and western sides (Figure 4e). There is

233   no incentive for the formation of tear faults in the sub-salt strata. This explains why

234   No. 7 Fault ends above the salt (Figure 4f).

235   **6 Discussion**

236   In 1980, Wheeler's primary research objective was to determine whether Parsons

237   and Petersburg Lineaments contained oil and gas (Wheeler, 1980). Similarly, for the

238   Tarim Basin, the direct significance of this study was to evaluate the ability of the tear

239   faults to connect with the deep source rock, namely, the Yuertusi Formation (Figure

240   1a). The NNE-SSW tear fault system is different from the NNW-SSE tear fault system.

241   The comparison between the two tear fault systems showed that the NNW-SSE

242   trending tear fault system did not penetrate salt; thus, it did not connect with deep

243   source rocks, which is important evidence for geologists engaged in the study of the

244   Tarim Basin.

245   Second, considering the development depth of tear faults, our results indicate that

246   the extraction of high-precision layered seismic attributes has a direct effect. However,

247   in the absence of good seismic data, the penetration of the tear fault into the salt can

248   be indirectly determined through the calculation of supra- and sub-salt strata

249   shortening. However, notably, if outcrop observations in an area with the development

250   of tear faults show evidence of compressive deformation in the sub-salt strata, or the

251   seismic interpretation of a single side of the tear fault shows evidence of deformation

252   in the sub-salt strata, we cannot directly conclude that the tear fault penetrated the salt.

253   Considering the example of No. 7 Fault, the sub-salt strata were compressed and

254   deformed, and Jura-type folds appeared beneath the salt (Figure 2m). However, as no

255   difference was observed in the shortening amount in different parts of the sub-salt

256   strata, No. 7 Fault still did not penetrate the salt. Therefore, the most critical basis for

257   evaluating whether a tear fault penetrates the salt is the difference in the thrust

258   displacement amount of the sub-salt strata on both sides of the fault, rather than

259   simply evaluating whether the sub-salt strata are compressed.

260   **7 Conclusion**

261   We extracted high-precision layered coherence maps in the seismic data covering

262   two tear faults, namely, Nos. 4 and 7 Faults, in Shuntuoguole Low Uplift and found

263   that No. 4 Fault penetrated the deep salt layer while No. 7 Fault did not. For No. 4

264 Fault, the strata shortening differences between the western and eastern sections exist

265 in both the supra- and sub-salt strata, whereas for No. 7 Fault, the strata shortening

266 differences only exist in the supra-salt strata. This result indicated that a tear fault

267 cannot penetrate the salt layer when there is no shortening difference in the sub-salt

268 strata, even though the sub-salt strata can be deformed during thrusting.

274 **Open Research**

275 **Data Availability Statement**

276 The seismic data supporting this research are owned by Sinopec, with commercial

277 restrictions, and are not accessible to the public or research community. The seismic

278 profiles used in this study is available at

279 https://doi.org/10.6084/m9.figshare.22197646.v1.

280 **References**

281 Bahorich, M., and Farmer, S., 1995, 3-D seismic discontinuity for faults and

282 stratigraphic features; the coherence cube: The Leading Edge, v. 14, p.

283 1053-1058.

284 Benesh, N.P., Plesch, A., and Shaw, J.H., 2014, Geometry, kinematics, and

285 displacement characteristics of tear-fault systems: An example from the

deep-water Niger Delta: AAPG Bulletin, v. 98, p. 465-482, doi:10.1306/06251311013.

Bian, Q., Deng, S., Lin, H., and Han, J., 2022, Strike-slip salt tectonics in the Shuntuoguole Low Uplift, Tarim Basin, and the significance to petroleum exploration: Marine and Petroleum Geology, v. 139, 105600.

Deng, S., Li, H., Zhang, Z., Zhang, J., Yang, X., 2019, Structural characterization of intracratonic strike-slip faults in the central Tarim Basin: AAPG Bulletin, v. 103, p. 109-137.

Deng, Q., Zhang, H., Wang, H., Wei, Z., Cheng, B., Li, S., Wang, Y., Faboya, O.L., and Liao, Z., 2021, Organic Matter Accumulation Mechanism in the Lower Cambrian Strata from Well Luntan 1 in the Tarim Basin, NW China: Geofluids, v. 4, p. 1-13.

Escalona, A., and Mann, P., 2006, Tectonic controls of the right-lateral Burro Negro tear fault on Paleogene structure and stratigraphy, northeastern Maracaibo Basin: AAPG Bulletin, v. 90, p. 479-504.

Fossen, H., 2010, Structural Geology: Cambridge, Cambridge University Press.

Gonzalez-Mieres, R., and Suppe, J., 2006, Relief and shortening in detachment folds: Journal of Structural Geology, v. 28, p. 1785-1807, doi:10.1016/j.jsg.2006.07.001.

Jackson, M.P.A., and Hudec, M.R., 2017, Salt tectonics: principles and practice: Cambridge, Cambridge University Press.

Jahani, S., Hassanpour, J., Mohammadi-Firouz, S., Letouzey, J., Frizon de Lamotte,

308   D., Alavi, A.S., and Soleimany, B., 2017, Salt tectonics and tear faulting in the

309   central part of the Zagros Fold-Thrust Belt, Iran: Marine and Petroleum Geology,

310   v. 86, p. 426-446, doi:10.1016/j.marpetgeo.2017.06.003.

311 Ji, T., Yang, W., Pu, R., and Wu, X., 2020, Research on the lithofacies and

312   paleogeography of the lower Cambrian Xiaoerbulake Formation in the northern

313   Tarim Basin, northwestern China: Canadian Journal of Earth Sciences, v. 57, p.

314   1463-1477.

315 Kang, Y., and Kang, Z., 1996, Tectonic evolution and oil and gas of Tarim Basin:

316   Journal of Southeast Asian Earth Sciences, v. 3, p. 317-325.

317 Laubscher, H.P., 1961, Die Fernschubhypothese der Jurafaltung: Eclogae Geologicae

318   Helvetiae, v. 54, p. 221-282.

319 Sun, Q., Fan, T., Gao, Z., Wu, J., Zhang, H., Jiang, Q., Liu, N., and Yuan, Y., 2021,

320   New insights on the geometry and kinematics of the Shunbei 5 strike-slip fault in

321   the central Tarim Basin, China: Journal of Structural Geology, v. 150, 104400.

322 Wheeler, R.L., 1980, Cross-Strike Structural Discontinuities: Possible Exploration

323   Tool for Natural Gas in Appalachian Overthrust Belt: AAPG Bulletin, v. 64, p.

324   2166-2178, doi:10.1306/2F91975B-16CE-11D7-8645000102C1865D.